Supporting Information

Near-Unity Absorption in Van der Waals Semiconductors for Ultrathin Optoelectronics

Deep Jariwala,[1,2] Artur R. Davoyan,[1,2,3] Giulia Tagliabue,[1,4] Michelle C. Sherrott,[1,2] Joeson Wong[1] and Harry A. Atwater[1,2,3,4]*

[1]Department of Applied Physics and Materials Science, California Institute of Technology, Pasadena, CA-91125, USA

[2]Resnick Sustainability Institute, California Institute of Technology, Pasadena, CA-91125, USA

[3]Kavli Nanoscience Institute, California Institute of Technology, Pasadena, CA-91125, USA

[4]Joint Center for Artificial Photosynthesis, California Institute of Technology, Pasadena, CA-91125, USA

*Corresponding author: haa@caltech.edu

S1. Absorbance calculations:

Absorption in ultrathin TMDCs on metals was calculated using the transfer matrix method.[1] The optical constants used for the calculation are the bulk crystal values for each TMDCs from previously published reports.[2, 3] Permittivities of Ag and Au were taken from Jhonson and Christie[4].

The maximum integrated absorbance in ultrathin TMDCs on a reflective metallic substrate is only achieved for a critical TMDC thickness which lies somewhere between 12-15 nm. Below this critical thickness, the absorption in the red part of the spectrum is reduced due to high reflection from the underlying metal. Above this thickness, the absorption in the blue part of the spectrum is reduced due to increased reflection from the TMDC owing to the mismatch in refractive index between air and the TMDC. Figure 2 c-d in the manuscript can be seen for experimental verification. The coupling of TMDCs with reflective metals is crucial for this resonantly enhanced absorption to occur. In case of a free standing WSe_2 of similar thickness, the total absorption is far lesser approaching ~40% between 6-12 nm thickness before falling down again due to increased reflection owing to index mismatch at the air /TMDC interface (Figure S1).

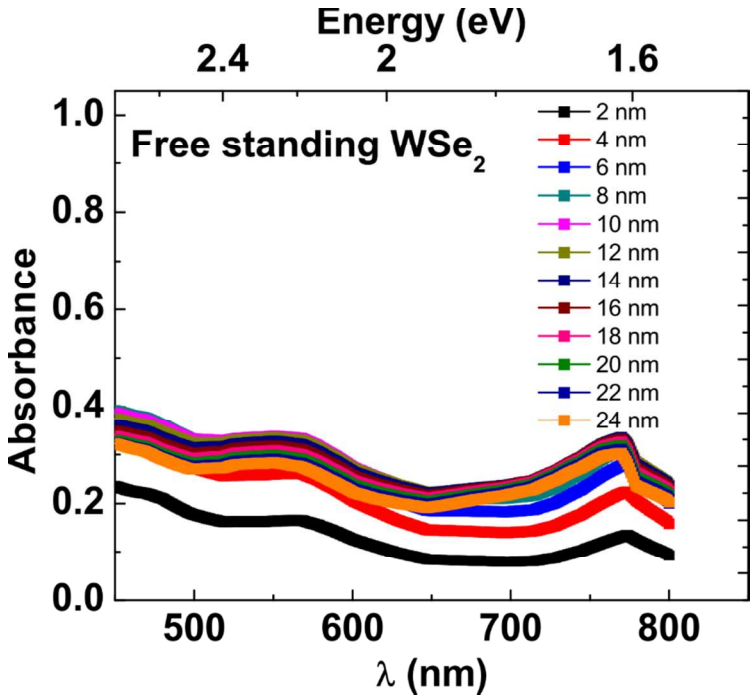

Figure S1: Calculated absorption in free standing WSe_2 with varying thickness. The total absorption increases with increasing thickness upto 12-14 nm and approaches ~40% following which it steadily drops down with further increase in the thickness.

S2. Absorption with Au back reflectors:

Figure S3 below shows calculated and measured absorption spectra for varying thicknesses of WSe_2 and WS_2 on template stripped Au back reflectors. A good qualitative and quantitative agreement between the measured and calculated spectra is apparent once again. However in Au, interband absorption starts dominating below 550 nm in wavelength. Therefore, the useful absorption in the TMDC layer (dashed lines) drastically reduces at $\lambda < 500$ nm. Ag back reflector is thus more suitable from an optical standpoint of maximizing useful absorption.

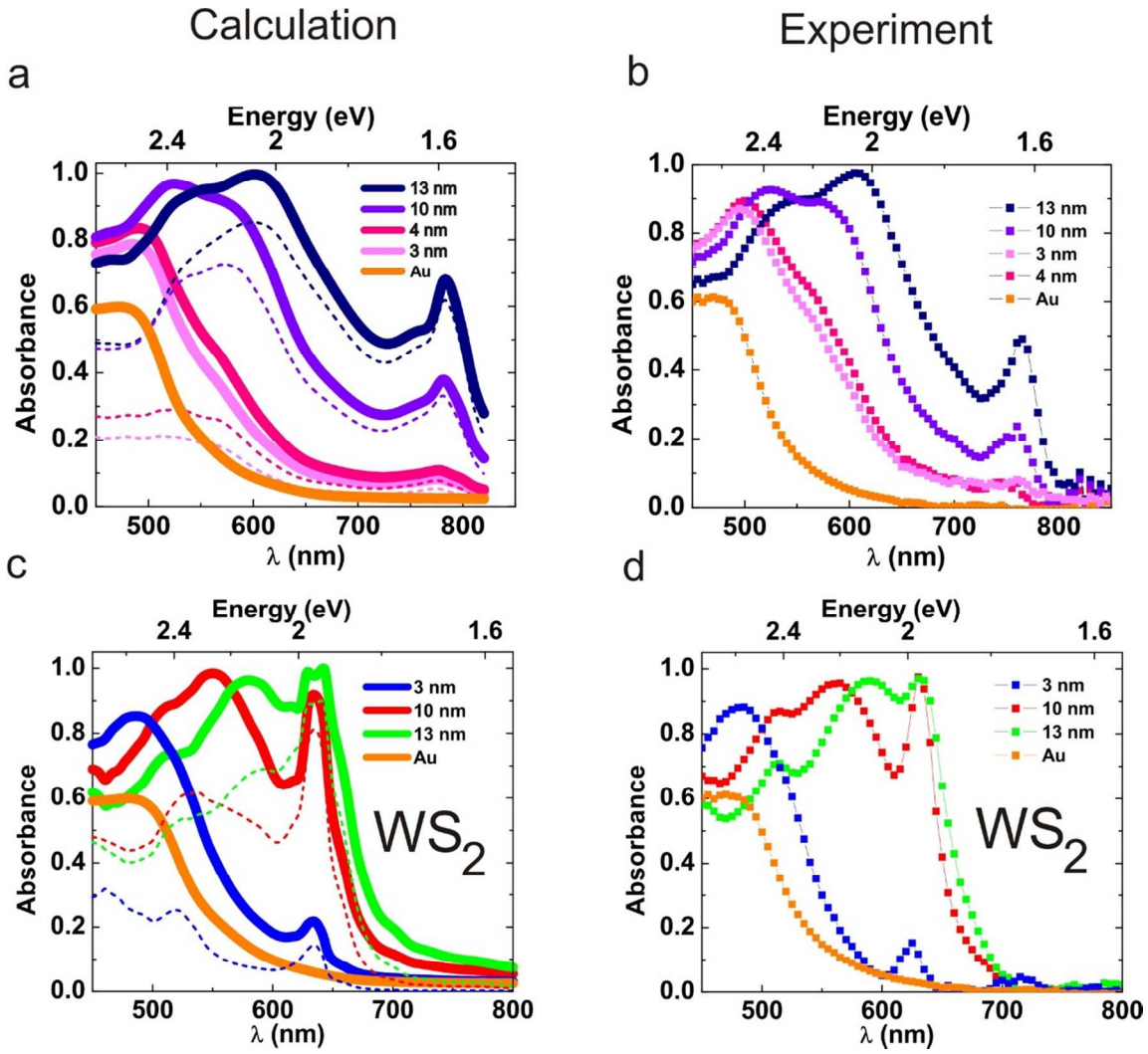

Figure S3: Calculated (left) and measured (right) absorption spectra of WSe_2 on Au (a-b) and WS_2 on Au(c-d).

S3. Estimation of minority carrier diffusion length.

Minority carrier diffusion length can be estimated from the spatial photocurrent profile. In cases where the diffusion length is larger than the spot size, a single exponential model $I = I_0\, exp(-x/L_D)$ where I is the photocurrent, I_0 is the peak photocurrent, x is the distance and L_D is the diffusion length can explain the photocurrent profile and provide an estimate of diffusion length. Considering that we are using a 633 nm laser for spatially resolving the photocurrent, the diffraction limited resolution (given by 0.61λ/N.A.), where N.A. is the numerical aperture of the objective, = 0.8 in our case) is ~500 nm in our measurement. Based on that, we can fit our photocurrent data to the above exponential decay equation and extract minority carrier diffusion lengths. We have estimated diffusion length varying from about 1.35 μm in Figure S4 a to about 3 μm in Figure S4 b.

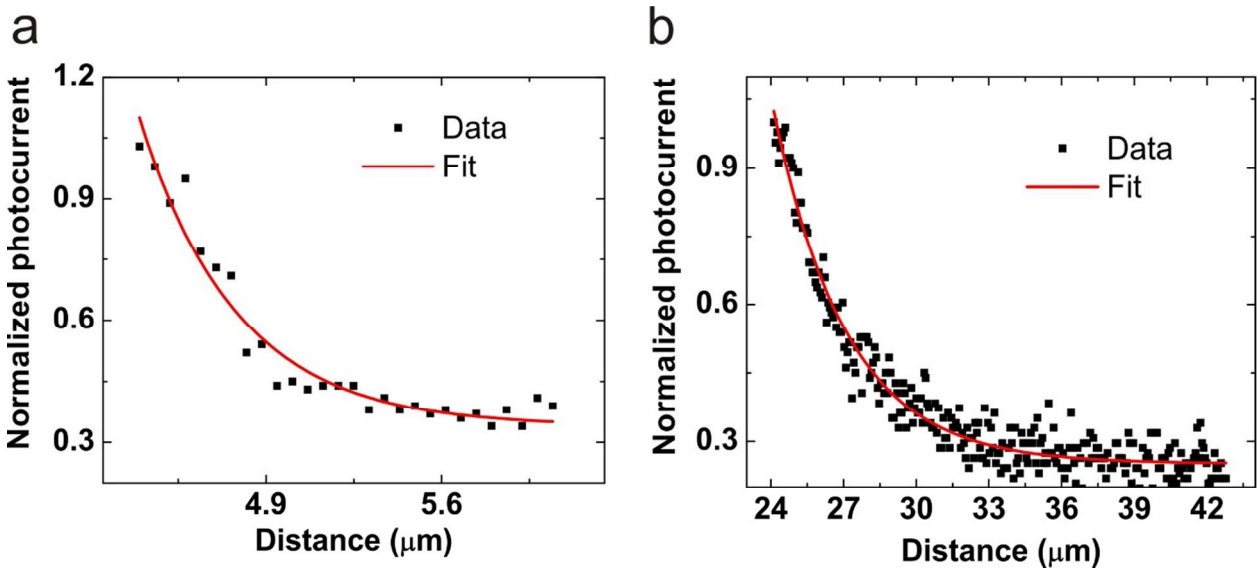

Figure S4. a. Photocurrent profile of device shown in Figure 3 e of the manuscript with a minority carrier diffusion length of ~1.35 μm b. Photocurrent profile of another representative device (19 nm WSe_2 on Au) shown in Figure 4 e of the manuscript with a minority carrier diffusion length of ~3 μm.

S4. Absorbance and EQE measurements:

A home-built optical set-up was used for both the absorption and EQE measurements. A supercontinuum laser (Fianium) coupled to a monochromator was used to provide the monochromated incident light. The collimated beam was focused onto the sample with a long working distance (NA = 0.55) 50x objective in order to achieve nearly normal illumination. The reflection spectrum was measured with a Si photodetector. Low noise signals were obtained by using a chopper and a lock-in amplifier. The measured reflection signal was then normalized to the reflection from a silver mirror (Thorlabs) in order to obtain the absolute reflection spectrum, $R(\lambda)$. In the absence of any transmission, the absorption spectrum can be obtained as $A(\lambda) = 1-R(\lambda)$.

The same illumination configuration was used for the EQE measurements. The photocurrent signal produced by the TMDC device was measured at each wavelength by mean of the chopper and lock-in amplifier. In addition, the power spectrum incident on the sample was later measured by placing the Si photodetector in the same position as the sample.

During all measurements, a small fraction of the illumination beam is deviated onto an optical fiber and sent to a second lock-in amplifier, also driven at the same frequency of the chopper. This reference signal is used to account for fluctuations of the illuminating beam over time enabling accurate normalization of the reflection and photocurrent signals.

S5. WS_2/WSe_2 heterojunctions:

Heterojunctions of few-layer WS_2/WSe_2 on Au substrates can also be fabricated by exfoliation and layer stacking using the dry transfer technique.[5] As compared to individual TMDC layers, heterojunctions show more enhanced, broadband absorption as shown below in Figure S5 below. Further since WS_2 and WSe_2 are known to form a type-II junction,[6] it is expected that the photocurrent collection efficiencies will also be enhanced in a optoelectronic device fabricated out of such heterojunctions with optimized layer thicknesses. Future work will involve fabricating metal ring contacts on such heterostructures and also fabricating graphene contacts to understand and enhance the carrier collection and open-circuit voltage in the resulting devices.

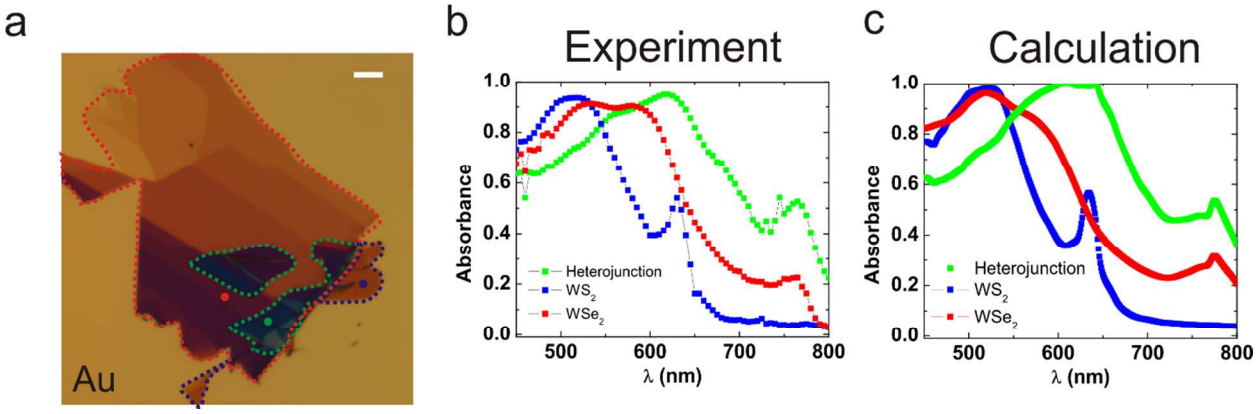

Figure S5: a. Optical micrograph of a $WS_2/WSe_2/Au$ heterostructure of varying thicknesses (scale bar = 5 μm). The blue, red and green boundaries indicate the WS_2/Au, WSe_2/Au and $WS_2/WSe_2/Au$ heterostructures regions respectively. The blue, red and green circles denote the spots from where the absorption spectra were acquired in b. b. Absorption spectra from the correspondingly colored circles in a. The layer thicknesses were measured using AFM. A clear increase in integrated absorption (area under the curve) is observed the case of heterojunction (green) vs individual WS_2 (blue) and WSe_2 (red) layers. c. Corresponding calculated spectra using the transfer matrix method in good agreement with the measurements in b.

References:

1. Born, M.; Wolf, E., *Principles of optics: electromagnetic theory of propagation, interference and diffraction of light*. Cambridge University Press: Cambridge, Unied Kingdom, 2000.
2. Li, Y.; Chernikov, A.; Zhang, X.; Rigosi, A.; Hill, H. M.; van der Zande, A. M.; Chenet, D. A.; Shih, E.-M.; Hone, J.; Heinz, T. F. *Phys. Rev. B* **2014,** 90, 205422.
3. Wilson, J. A.; Yoffe, A. D. *Advances in Physics* **1969,** 18, 193-335.
4. Johnson, P. B.; Christy, R. W. *Phys. Rev. B* **1972,** 6, 4370-4379.
5. Andres, C.-G.; Michele, B.; Rianda, M.; Vibhor, S.; Laurens, J.; Herre, S. J. v. d. Z.; Gary, A. S. *2D Mater.* **2014,** 1, 011002.
6. Wang, K.; Huang, B.; Tian, M.; Ceballos, F.; Lin, M.-W.; Mahjouri-Samani, M.; Boulesbaa, A.; Puretzky, A. A.; Rouleau, C. M.; Yoon, M.; Zhao, H.; Xiao, K.; Duscher, G.; Geohegan, D. B. *ACS Nano* **2016**, 10.1021/acsnano.6b01486.